Journal of Biomechanics 47 (2014) 847–858

Contents lists available at ScienceDirect

Journal of Biomechanics

journal homepage: www.elsevier.com/locate/jbiomech
www.JBiomech.com

Plaque hemorrhage in carotid artery disease: Pathogenesis, clinical and biomechanical considerations

Zhongzhao Teng [a,b,*], Umar Sadat [c], Adam J. Brown [d], Jonathan H. Gillard [a]

[a] University Department of Radiology, University of Cambridge, UK
[b] Department of Engineering, University of Cambridge, UK
[c] Department of Surgery, Cambridge University Hospitals NHS Foundation Trust, UK
[d] Department of Cardiovascular Medicine, University of Cambridge, UK

ARTICLE INFO

Article history:
Accepted 13 January 2014

Keywords:
Carotid
Atherosclerosis
Atheroma
Stroke
Hemorrhage
Mechanics
MRI

ABSTRACT

Stroke remains the most prevalent disabling illness today, with internal carotid artery luminal stenosis due to atheroma formation responsible for the majority of ischemic cerebrovascular events. Severity of luminal stenosis continues to dictate both patient risk stratification and the likelihood of surgical intervention. But there is growing evidence to suggest that plaque morphology may help improve pre-existing risk stratification criteria. Plaque components such a fibrous tissue, lipid rich necrotic core and calcium have been well investigated but plaque hemorrhage (PH) has been somewhat overlooked. In this review we discuss the pathogenesis of PH, its role in dictating plaque vulnerability, PH imaging techniques, marterial properties of atherosclerotic tissues, in particular, those obtained based on in vivo measurements and effect of PH in modulating local biomechanics.

1. Introduction

Carotid artery disease is responsible for about 30% of ischemic strokes (Levy et al., 2008), which is the third leading cause of mortality and the primary cause of disability in developed countries (Roger et al., 2011). Currently, carotid luminal stenosis is the only validated diagnostic criterion for clinical risk stratification. Large multicentre clinical trials have shown that carotid endarterectomy (CEA) provides maximum benefit to patients with a significant carotid stenosis ($\geq$70%) (Barnett et al., 1998). The overall risk-to-benefit ratio for CEA however becomes marginal in patients with moderate stenosis (50–69%). Since patients with moderate carotid stenosis constitute the majority of individuals suffering from clinical events (Barnett et al., 1998; Rothwell et al., 2003), there is therefore a need to identify better risk stratification tools besides luminal stenosis.

The primary mechanism for an ischemic stroke due to carotid atherosclerotic disease is believed to be an embolic event from a ruptured carotid plaque (Rothwell et al., 2000). As a multi-component structure, plaque stability is determined by both its structure and local haemodynamics, including arterial pressure and flow. A typical carotid atherosclerotic plaque is composed of lipid-rich necrotic core (LRNC), plaque hemorrhage (PH) and calcium, all covered by an overlying fibrous cap (FC). Large LRNC with or without PH and thin FC characterize a high-risk plaque. Although plaque components such as LRNC, FC and calcium have been extensively studied, PH has been much less investigated. There is growing evidence that PH is critical in dictating plaque vulnerability and is associated with subsequent ischemic events (Kolodgie et al., 2003; Michel et al., 2011; Sadat et al., 2010b). PH has been observed to be more prevalent in acutely symptomatic patients than in asymptomatic individuals (Imparato et al., 1983; Sadat et al., 2009), while prospective studies have confirmed that PH confers additional risk in both symptomatic and asymptomatic patients (Altaf et al., 2008, 2007; Eliasziw et al., 1994; Sadat et al., 2010b; Singh et al., 2009; Takaya et al., 2006).

Compositional features provide complementary information to luminal stenosis in carotid plaque vulnerability assessment. Indeed, about 60% symptomatic patients exhibit PH or FC rupture at baseline (Gao et al., 2007; Milei et al., 2003), yet only 10–20% will go on to experience a recurrent event at 1 year (Sadat et al., 2010b; U-King-Im et al., 2009). It is therefore clear that composition alone cannot serve

Abbreviations: ΔHU, density difference of Hounsfield (a quantitative scale for describing radiodensity); 2D, two dimensional; 3D, three dimensional; CEA, carotid endarterectomy; CT, computerized tomography; CTA, computerized tomography angiography; FC, fibrous cap; FSE, fast spin echo; FSI, fluid–structure interaction; FTIR, Fourier transform infrared; LRNC, lipid-rich necrotic core; MIP, maximum intensity projection; MRI,, magnetic resonance image; PH, plaque hemorrhage; SEDF, strain energy density functions; SHINE, Sequence for Hemorrhage assessment using INversion recovery and multiple Echoes; SNAP, Simultaneous Noncontrast Angiography and intraPlaque hemorrhage; SPI, slab-selective phase-sensitive inversion-recovery; TOF, time-of-flight

* Correspondence to: University Department of Radiology, University of Cambridge, Level 5, Box 218, Addenbrooke's Hospital, Hills Road, Cambridge CB2 0QQ, UK. Tel.: +44 1223 746447; fax: +44 1223 330915.
E-mail address: zt215@cam.ac.uk (Z. Teng).

0021-9290/$ - see front matter © 2014 Elsevier Ltd. Open access under CC BY-NC-ND license.
http://dx.doi.org/10.1016/j.jbiomech.2014.01.013

as a marker for prospective cerebrovascular risk and there is a need to identify novel biomarkers. Under the physiological conditions, carotid plaques are subjected to mechanical loading driven by pulsatile blood pressure. FC rupture may occur when this loading exceeds its material strength. Therefore, a strategy integrating both high risk anatomical plaque features and mechanical conditions may improve patient risk stratification and ultimately guide clinical treatment. With this consideration, this review will focus on (1) the pathological features of PH and its clinical significance; (2) the non-invasive in vivo imaging techniques used to depict PH; (3) the material properties of atherosclerotic components, including PH; and (4) the critical mechanical conditions within a hemorrhagic plaque.

2. Pathology of plaque hemorrhage and clinical significance

2.1. Plaque hemorrhage and associated neovascularization

The involvement of hemoglobin-rich plaque hemorrhage in the transformation of a stable to unstable atherosclerotic lesion was proposed as early as 1936 (Paterson, 1936). At the same time it was suggested that rupture of neovessels could be the initiating event for PH (Paterson, 1938; Wartman, 1938). After this initial period, the clinical and biological significance of PH became rather overlooked. The majority of biological studies focussed on either lipid metabolism or the inflammatory response within the plaque. Imparato et al. (1979) reported the relationship between PH observed in CEA samples and neurological symptoms. Since then various studies have assessed this relationship which are summarized by Gao et al. (2007). Others have investigated the relationship between PH and plaque neovessels (Fryer et al., 1987; McCarthy et al., 1999). Observations that erythrocyte extravasation and PH are related to high density of plaque neovessels, in the absence of plaque fissuring, support the common viewpoint that PH is related to neovessels leakage (Virmani et al., 2005), due to leaky endothelial junctions (Jeziorska and Woolley, 1999) (Fig. 1). An alternate viewpoint is that repeated plaque fissuring and associated formation of non-occlusive luminal thrombus gets incorporated into the plaque (Davies and Thomas, 1985). Either way, the extracorpuscular hemoglobin released following the phagocytosis of red blood cells in PH acts as a pro-inflammatory agent, promoting local inflammation (Fig. 2) and plaque progression (Moreno et al., 2012). PH also carries proteolytic enzymes, causing thinning of the FC and making the plaque liable to rupture (Michel et al., 2012). Readers are directed to other excellent articles (Levy and Moreno, 2006; Michel et al., 2011) for further relevant pathological details, as they are beyond the scope of this review.

2.2. Prevalence of plaque hemorrhage (PH) in patients with carotid artery disease

The prevalence of PH in symptomatic and asymptomatic patients has been mostly obtained from ex vivo histological examination of CEA or cadaveric tissue. In the 29 histological studies (Table 1) including both symptomatic and asymptomatic

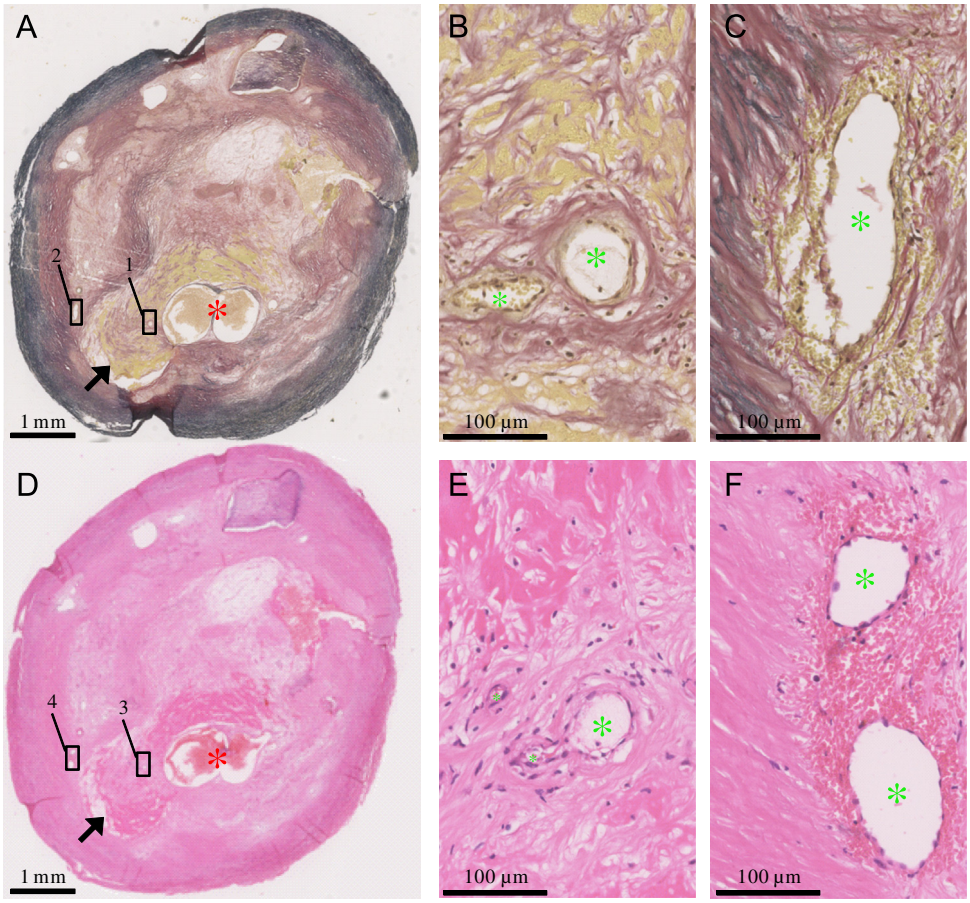

Fig. 1. Atherosclerotic plaque sample collected from carotid endarterectomy of a 72-year old symptomatic patient (male) showing both old thrombus and plaque hemorrhage around neovessels: (A and D) Van Gieson's (EVG) and Hematoxylin and eosin (HE) stains showing elastin (black in EVG), collagen (pink in HE) and erythrocyte and its debris (brown in EVG and red in HE); (B and E) local views of 1 in (A) and 3 in (B) showing neovessels in a old thrombus resulted from previous rupture (marked by arrow in A and D); (C and F) local views of 2 in (A) and 4 in (B) showing erythrocytes (fresh plaque hemorrhage) around neovessels; red asterisk: arterial lumen; green asterisk: the lumen of neovessels. (For interpretation of the references to color in this figure legend, the reader is referred to the web version of this article.)

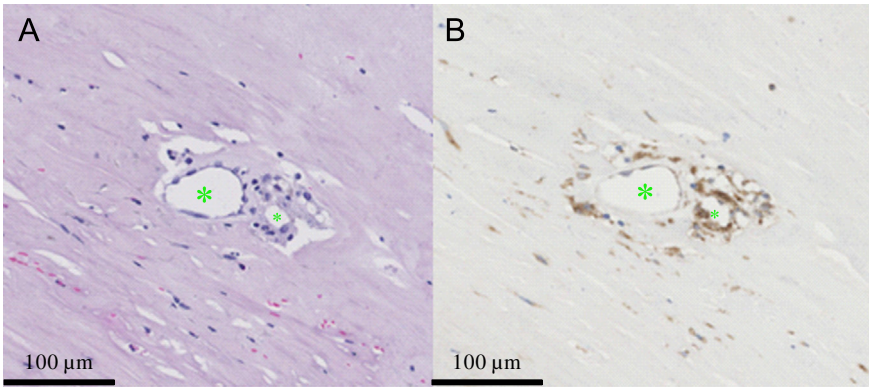

Fig. 2. Aggregation of macrophages around neovessels (A) hematoxylin and eosin (HE) stain showing neovessels within a fibrotic region; (B) CD68 stain showing the surrounding macrophages; green asterisks: lumens of neovessels. (For interpretation of the references to color in this figure legend, the reader is referred to the web version of this article.)

Table 1
The prevalence of histologically identified plaque haemorrhage (PH) in symptomatic and asymptomatic patients.

Reference (year)	Symptomatic			Asymptomatic			*p*-Value
	PH (%)	PH (*n*)	Patient (*n*)	PH (%)	PH (*n*)	Patient (*n*)	
Lusby et al. (1982a)	92.5	49	53	26.9	7	26	< 0.0001
Reilly et al. (1983)	73.0	27	37	53.8	7	13	0.354
Persson et al. (1983)	97.1	33	34	52.4	11	21	0.0002
Ammar et al. (1984)	90.9	40	44	78.1	25	32	0.218
Persson (1986)	95.0	93	98	61.3	38	62	< 0.0001
Ricotta et al. (1986)	76.5	26	34	23.5	8	34	< 0.0001
Ammar et al. (1986)	95.5	42	44	78.1	25	32	0.051
Lennihan et al. (1987)	45.9	56	122	52.6	40	76	0.439
Fryer et al. (1987)	81.7	58	71	45.0	9	20	0.003
Bassiouny et al. (1989)	67.7	21	31	85.7	12	14	0.368
AbuRahma et al. (1990)	60.4	61	101	9.4	5	53	< 0.0001
Bornstein et al. (1990)	85.9	61	71	83.3	5	6	0.663
Sterpetti et al. (1991)	68.2	30	44	37.3	25	67	0.003
von Maravic et al. (1991)	93.3	14	15	91.3	21	23	0.699
Feeley et al. (1991)	56.8	25	44	37.5	3	8	0.532
Arapoglou et al. (1994)	77.2	44	57	37.5	12	32	0.0005
Fisher et al. (1994)	53.1	17	32	72.6	45	62	0.098
Sitzer et al. (1995)	22.2	6	27	7.4	2	27	0.251
Seeger et al. (1995)	47.7	10	21	54.5	12	22	0.888
Carr et al. (1996)	84.2	16	19	56.0	14	25	0.096
Bassiouny et al. (1997)	18.6	11	59	17.5	7	40	0.920
Milei et al. (1998)	50.6	43	85	51.3	41	80	0.920
Montauban van Swijndregt et al. (1999)	93.9	31	33	71.4	10	14	0.101
McCarthy et al. (1999)	61.5	8	13	20.0	3	15	0.063
Tegos et al. (2000)	67.4	31	46	76.0	19	25	0.624
Milei et al. (2003)	23.3	31	133	29.1	43	148	0.340
Turu et al. (2006)	49.1	27	55	37.9	11	29	0.454
Hellings et al. (2010)	72.8	484	665	69.9	107	153	0.543
Derksen et al. (2011)	81.4	542	666	79.7	102	128	0.740

χ^2 test in R 2.10.1 (The R Foundation for Statistical Computing) was used for the statistical analysis and significant difference was assumed if $p < 0.05$.

Table 2
MRI-depicted plaque haemorrhage (PH) in symptomatic and asymptomatic patients/sides.

Reference (year)	Symptomatic			Asymptomatic			*p*-value
	PH (%)	PH (*n*)	Patient (*n*)	PH (%)	PH (*n*)	Patient (*n*)	
Saam et al. (2006)[a]	100.0	23	23	87.0	20	23	0.232
U-King-Im et al. (2008)	44.4	8	18	15.8	3	19	0.122
Sadat et al. (2009)	45.0	18	40	5.0	1	20	0.004
DeMarco et al. (2010)[b]	67.0	4	6	25.0	11	44	0.106
DeMarco et al. (2010)[c]	43.0	3	7	36.0	12	33	0.920
Cheung et al. (2011)[a]	13.0	31	217[d]	7.0	14	217[e]	0.045
Turc et al. (2012)	33.0	38	114	31.0	37	120	0.791
Lindsay et al. (2012)	22.0	9	41	15.0	6	40	0.603
Qiao et al. (2012)	62.5	15	24	30.4	7	23	0.056
Millon et al. (2013)	39.0	20	52	16.0	16	102	0.003
Grimm et al. (2013)	67.6	23	34	11.8	4	34	< 0.0001

χ^2 test in R 2.10.1 (The R Foundation for Statistical Computing) was used for the statistical analysis and significant difference was assumed if $p < 0.05$.

[a] Bilateral studies.
[b] Mild to moderate luminal stenosis.
[c] Severe luminal stenosis.
[d] 233 Plaques.
[e] 201 Plaques.

patients, PH was reported to range from 18.6% to 97.1% (median [inter quartile range (IQR)]: 72.8% [53.1, 85.9]) in symptomatic patients and from 7.4% to 91.3% (52.6% [37.3, 72.6]) in asymptomatic patients. Eight studies showed that PH had a higher prevalence in symptomatic patients; however 21 studies found no difference in PH prevalence between patient groups. Importantly none of studies conducted after 1995 found a difference in the rates of PH. This could be a result of preventive treatment (including statins), which came into widespread clinical use around this time. Nevertheless, if data were pooled, PH was more prevalent in symptomatic compared to the asymptomatic patients [70.3% (1937 out of 2754) vs. 52.0% (669 out of 1287); $p < 0.0001$].

High resolution, multi-contrast MRI has been shown to be the most promising technique to depict PH with the sensitivity and specificity being $89.7 \pm 6.8\%$ and $85.6 \pm 9.1\%$ respectively (Bitar et al., 2008; Chu et al., 2004; Kampschulte et al., 2004; Moody et al., 2003; Ota et al., 2010; Qiao et al., 2011; Yim et al., 2008). MRI-based clinical studies (Table 2) have confirmed that PH has a higher prevalence in symptomatic lesions (symptomatic 33.3%; 192/576 vs. asymptomatic 19.4%; 131/675; $p < 0.0001$). This suggests a potential role of PH in the etiology of stroke. It is only through well designed future studies, with uniformity in the definition and evaluation of PH, that the full mechanism will be elucidated (Gao et al., 2007).

2.3. Association between plaque hemorrhage (PH) and plaque progression

As stated earlier, PH is known to promote plaque progression. In an 18-month follow-up study of asymptomatic patients with 50–70% luminal stenosis, percentage change in wall volume and lipid-rich necrotic core volume was significantly higher in the group of patients with PH (Takaya et al., 2005). Those with PH at baseline were also more likely to have new PH at 18 months compared to controls (43% vs. 0%; $p = 0.006$). This finding was consistent with that of Spagnoli et al. (2004) who had observed

Table 3
The risk nature of plaque haemorrhage in symptomatic patients with mild to moderate luminal stenosis (30–69%).

Reference (year)	Patients (n)	Hazard ratio (HR)	95% Confident interval (CI)	p-Value	Follow-up period	Description
Altaf et al. (2008)	64	9.8	1.3-75	0.03	28 [26–30] months	13 recurrent events occurred in 39 arteries with IPH.
Sadat et al. (2010c)	61	5.85	1.27-26.77	0.02	514 [255–718] days	–
Teng et al. (2011)	21	–	–	–	262 [10–610] days	11 patient with juxtaluminal haemorrhage/thrombus experienced recurrent events.
Kurosaki et al. (2011)	34	–	–	–	Mean 9.1 months	5 patients experienced recurrent ischemic events.
Yoshida et al. (2012)	25	–	–	–	31.3±16.4 months	11 patients developed a total of 30 recurrent ischemic events.
Kwee et al. (2013)	126	3.542	1.058-11856	0.04	One year	-

fresh thrombus in carotid plaques from CEA samples of patients, up to 24 months after an ischemic stroke. In a long-term (54 months) follow-up study, the development of PH was found to have a marked effect on plaque progression (Sun et al., 2012). A multicentre study with 6-month follow-up corroborated these results (Sun et al., 2013). Although a few studies have failed to show association between PH and plaque progression (Kwee et al., 2012, 2010), they did surprisingly reported an association between PH and recurrent cerebrovascular events (Kwee et al., 2013).

2.4. Association between plaque hemorrhage (PH) and subsequent ischemic events

Atherosclerotic disease progresses over decades (slow progression) but can, under certain circumstances, lead to acute symptomatic events (rapid progression) (Fuster, 1994; Kiechl and Willeit, 1999). The presence of PH can be a contributing factor (Lusby et al., 1982a, 1982b). In a longitudinal MRI study involving 154 asymptomatic patients with 50–79% luminal stenosis, PH was observed to increase the risk of subsequent ischemic cerebrovascular events by five times during a mean follow-up period of 38.2 months (Takaya et al., 2006). The authors highlighted that the ability to distinguish LRNC with PH plaque from the one without PH was critical in identifying higher risk patients. In a complementary study, six cerebrovascular events occurred in 36 asymptomatic patients (50%–70% luminal stenosis) with PH, whilst no clinical events occurred in the 39 patients without PH during a mean follow-up of 24.9 months (Singh et al., 2009). Other investigators have found a similar association between PH and subsequent ischemic events (Altaf et al., 2007; Kurosaki et al., 2011), but not always (Sun et al., 2012). Recently, Hosseini et al. (2013) reported 63.7% of hemorrhage prevalence in 179 symptomatic patients with $\geq$50% luminal stenosis and 92% (57 out 62) patients who showed PH suffered recurrent ipsilateral events. The risk of recurrent clinical events in symptomatic patients with PH and mild to moderate (30–69%) luminal stenosis has been tabulated in Table 3.

3. Imaging modalities for assessing focal carotid plaque hemorrhage (PH)

3.1. Ultrasonography

Ultrasound imaging allows qualitative and quantitative analysis of carotid plaque. It has the ability to identify the location, internal characteristics, and surface detail of plaque adequately. Ultrasonography identifies two plaque categories based on the heterogeneous and homogeneous echo patterns of the lesion studied (Reilly et al., 1983). However, at present it is unable to give detailed morphometric information regarding plaque components such as FC thickness and PH age, known important features of plaque vulnerability. Furthermore, ultrasound is unable to provide sufficient information about the underlying pathological processes involved in atherosclerosis, including inflammatory neovascularization. Ultrasonic contrast agents have been introduced to improve image resolution and specificity (Demos et al., 1999; Lindner et al., 2000). They have shown promising results in various feasibility studies in identifying the inflammatory neovessels in carotid atheroma (Coli et al., 2008; Vicenzini et al., 2007), but this methodology is still in its infancy and will require significant further development before translation into clinical practice.

3.2. Computerized tomography (CT)

With the recent advent of multi-slice computerized tomography (CT) technology, high resolution imaging in the arterial phase of arteries from the aortic arch to the skull base can be rapidly acquired. From the axial source images, image post-processing can be performed to produce an angiographic display, identifying plaque calcium, luminal surface ulceration (Saba et al., 2007; U-King-Im et al., 2010) and intraluminal thrombus (Eesa et al., 2010). However, limitations of CT and CT angiography (CTA) include exposure to ionizing radiation in addition to artefacts induced by calcification and implanted metallic devices. Moreover, CT angiography cannot depict plaque soft components (Walker et al., 2002), including PH, due to the wide distribution of CT density (U-King-Im et al., 2010). With improved technology such as multi-slice detector-rows or dual energy CT (DECT) machines, the accuracy of CTA in depicting soft atherosclerotic content may be further increased. DECT has been reported to improve the ex vivo differentiation between soft tissues (Zachrisson et al., 2010). Results from 31 patients indicated that multidetector CT showed a high level of sensitivity and a moderate level of specificity in detecting atherosclerotic carotid plaques complicated with hemorrhage (Ajduk et al., 2009). It was found that the density difference (ΔHU) between early and delayed phases was associated with tissue type in carotid plaques. Histology confirmed that ΔHU was positively correlated with fibrous tissue and negatively correlated with a lipid-rich necrotic core with hemorrhage (Horie et al., 2012). However, further studies are needed for confirmation of these promising results.

3.3. Magnetic resonance imaging (MRI)

High resolution, multi-contrast MRI has shown a great capacity in depicting various atherosclerotic components within carotid plaques (Gortler et al., 1995; Toussaint et al., 1996; Underhill et al., 2010). Detection of plaque hemorrhage by carotid MRI relies on the degradation of hemorrhage into magnetic susceptible hemosiderin and ferritin, two iron-storing proteins present in macrophages, which shorten the longitudinal relaxation time (T_1) of surrounding protons. The consequent imaging effect in carotid MR

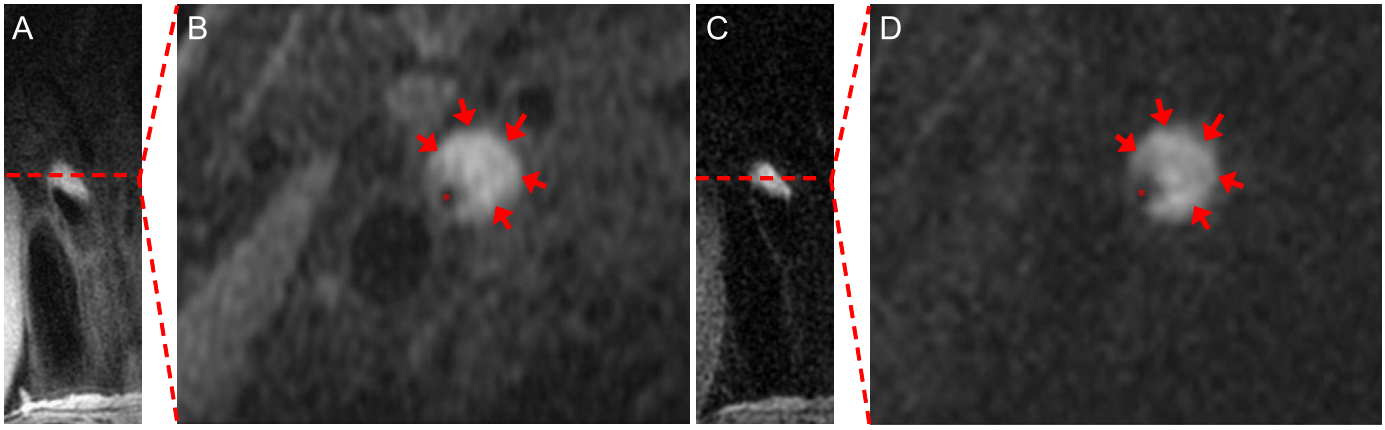

Fig. 3. A large plaque hemorrhage depicted by MR imaging from a 72-year old asymptomatic patient (A) and (B) 3D-CUBE T_1-weighted MR image in coronal and transverse planes; (C) and (D) direct thrombus image (DTI) at the same location in (A) in coronal and transverse planes; red asterisk: arterial lumen. (For interpretation of the references to color in this figure legend, the reader is referred to the web version of this article.)

imaging is a bright signal on T_1-weighted sequences such as time-of-flight (TOF) and standard T_1-weighted fast spin echo (FSE) sequences (Fig. 3A), with low signal intensity in T_2-weighted sequences. These sequences have been extensively validated with histology (Chu et al., 2004; Kampschulte et al., 2004; Toussaint et al., 1996; Yuan et al., 2001). TOF maximum intensity projection (MIP) images have high overall specificity [100.0%, 95% confident interval (CI): 93.0–100.0%], but relatively low sensitivity (32%, 95% CI: 20.8–47.9%) for the identification of PH (Yamada et al., 2012). Contrast enhanced-MR angiography has been suggested as a method to improve the sensitivity in PH detection, when compared to TOF sequence (Qiao et al., 2011).

PH identified on MRI can also be described according to location; intraplaque when the FC is intact and juxtaluminal when there is luminal extension to the thrombus. TOF pulse sequence is particularly helpful in this description (Kampschulte et al., 2004). Juxtaluminal hemorrhage is characterized by discontinuity of dark band in TOF (indicating FC rupture) and high signal intensity in T_1-weighted image, while intraplaque hemorrhage has a smooth luminal contour (Kampschulte et al., 2004; Teng et al., 2011). PH can also be classified according to time of formation, either as fresh/acute (<1 week), recent (1–6 weeks) or remote/old (>6 weeks) (Lusby et al., 1982a). Fresh hemorrhage or thrombus has a shorter T_2 (Toussaint et al., 1996) appearing hypointense in T_2-weighted images. Following PH organization, the intensity of the susceptibility effect is diminished, appearing hyperintense on T_2-weighted images. Old (or remote) hemorrhage appears hypointense in all TOF, T_1- and T_2-weighted images (Chu et al., 2004).

As the pathological and clinical importance of PH has become established, efforts have been made on developing more efficient MR sequences for PH identification. Direct thrombus imaging (DTI), a T_1-weighted MR sequence, has been widely used to depict PH by suppressing the fat signal normally seen on T_1-weighted sequences (Fig. 3B). It does not however provide information about the location or age of PH (Chu et al., 2004). A 3-dimentional (3D) T_1-weighted magnetization prepared rapid acquisition gradient echo (MPRAGE) sequence (Mugler and Brookeman, 1990) has been introduced to detect PH with a bigger contrast-to-noise ratio, improving both sensitivity and specificity (Ota et al., 2010). An optimized 3D spoiled gradient recalled echo pulse Sequence for Hemorrhage assessment using INversion recovery and multiple Echoes (3D SHINE) has been developed to differentiate between fresh and recent PH (Zhu et al., 2010). To further improve intraplaque hemorrhage to wall contrast with suppression of blood signal, a slab-selective phase-sensitive inversion-recovery (SPI) technique is proposed (Wang et al., 2010). A simultaneous non-contrast angiography and PH (SNAP) MR imaging technique was also proposed recently to image both lumen size and carotid PH in a single scan (Wang et al., 2013). Nonetheless, MR offers the most detailed assessment of PH in humans, in terms of its location within a plaque and its age, whilst also offering ability to have a detailed concomitant assessment of other high-risk plaque features.

4. Local biomechanical stresses and carotid plaque hemorrhage

Since carotid plaques are located at the location of the carotid artery bifurcation, the effect of structural biomechanical stresses cannot be overlooked. The biomechanical forces acting on a plaque, which is weakened structurally by the underlying inflammation driven by agents like PH (Altaf et al., 2013), can trigger plaque rupture due to excess loading on the thin FC. Although this remains a hypothesis, circumstantial evidence supports this mechanism. Due to the close relationship between plaques and local haemodynamics, the integration of plaque morphology and mechanical analysis has the potential to improve plaque vulnerability assessment.

For a successful mechanical analysis, knowledge of several important variables is required including governing equations, material properties, geometrical determinants, loading and boundary conditions. In particular, the material behavior of various plaque components, such as FC, lipid and PH are necessary for the accuracy. Moreover, other pre-processing procedures such as geometric reconstruction, the shrinkage procedure and mesh generation are involved. As these components of the simulation are essential they shall be discussed in detail.

4.1. General aspects in biomechanical analysis with carotid plaques

Plaque is a multi-component structure with irregular geometries. The material properties of each component are highly non-linear. The entire plaque undergoes a large deformation due to blood pressure and flow, while the governing equations describing the motion are non-linear. These properties make the mechanical analysis complex, particularly when both plaque structure and blood flow are considered in a computational model [i.e., fluid–structure interaction model (FSI)].

The mechanical properties of atherosclerotic tissues are usually from ex vivo direct material measurements. However this approach is short of clinical potential. Elastography (de Korte et al., 2002; Hu et al., 2011; Shi et al., 2008; Zhang et al., 2010a, 2010b) has been

developed to quantify the material properties of plaque using in vivo data. Some numerical techniques have been also developed for similar purposes (Liu et al., 2012; Schulze-Bauer and Holzapfel, 2003). An accurate measurement of geometric determinants, including FC thickness, LRNC size and lumen curvature, is essential for an accurate numerical prediction. Accuracy is further determined by the imaging resolution, which clearly depends on the imaging technique chosen. For MR carotid imaging, the resolution is determined by the magnetic strength, number of coil element arrays and imaging parameters. The resolution of traditional 2D turbo sequences usually is $0.39\times0.39\times2$(or 3)mm^3 (Fuster et al., 2005; Trivedi et al., 2004) with an anatomical coverage of 15–30 mm. It can be improved to about $0.5\times0.5\times1\ mm^3$ with much larger coverage up to 100–150 mm using newly developed 3D isotropic sequences (Balu et al., 2011, 2009; Li et al., 2010). Such improvement is beneficial for a more accurate geometric reconstruction. Loading conditions include arterial blood pressure and velocity. Non-invasive central blood pressure measurements (carotid artery and thoracic aorta) have been developed and widely validated for this purpose (Papaioannou et al., 2009; Siebenhofer et al., 1999). Blood velocity can be quantified using phase contrast MR imaging (Gatehouse et al., 2005; Long et al., 2000). Residual stress exists in the arterial wall and atherosclerotic structure, but this cannot be accounted for using imaging alone. The influence of residual stress on the carotid bifurcation (Delfino et al., 1997) and atherosclerotic structure (Ohayon et al., 2007) has been previously quantified.

The central issue is in the modeling of the plaque. Different strategies have been adopted to predict stress within the plaque structure. The most comprehensive could be the full coupled 3D FSI simulation (Bluestein et al., 2008; Leach et al., 2010; Tang et al., 2009b). Considering the difficulty of convergence, one-way 3D FSI (Gao et al., 2009) and 2D FSI (Kock et al., 2008; Thrysoe et al., 2010) have been used as alternatives. 3D (Kiousis et al., 2009; Teng et al., 2011) and 2D (Sadat et al., 2011a; Tang et al., 2009a) structure-only modeling have also been used for population based analyses. Tang et al. (2009a) showed a similar stress distribution pattern between 3D full coupled FSI and 2D structure-only analysis using data from one patient. How much the results of each model differ from another awaits comprehensive comparison.

4.2. Material properties of atherosclerotic tissue

4.2.1. Derived from ex vivo direct measurements

The direct material measurement with human atherosclerotic tissues is very limited; readers are referred to summaries on the direct measurements with atherosclerotic tissue in the following references (Chai et al., 2013; Sadat et al., 2010a). In recent years, a few ex vivo direct measurements within carotid tissues have been reported. Fourier transform infrared (FTIR) spectroscopy was used to quantify the amount of mineral and lipid in each tissue region then tested ($n=10$) (Ebenstein et al., 2009). The results demonstrated that the stiffness of plaque tissue increases with increasing mineral content. Maher et al. (2009) tested fresh CEA samples ($n=14$). Their results indicated that calcified plaques had the stiffest response, while echolucent plaques were the least stiff. Holzapfel's group has performed direction and layer-specific studies in both normal and atherosclerotic carotid tissues on the residual strain and material properties (Sommer et al., 2010; Tong et al., 2011). By testing the whole plaque sample ($n=14$) in its entirety, it was found that experimental Green strains at rupture varied from 0.299 to 0.588 and the Cauchy stress observed in the experiments was between 0.131 and 0.779 MPa (Lawlor et al., 2011). Biaxial test has also been employed to characterize the anisotropic behavior of diseased carotid arteries ($n=5$) using planar biaxial testing (Kural et al., 2012).

Some studies treat plaque tissue as a linear elastic material (Cheng et al., 1993; Loree et al., 1994), in particular those based on in vivo measurements (see next section). Most material models assume each type of tissue, including FC and healthy media, as non-linear, hyper-elastic, homogeneous and incompressible. Various strain energy density functions (SEDF) have been used to describe the material behavior of carotid atherosclerotic tissues, treating the tissue to be either isotropic or anisotropic. The following SEDFs can be found in literature; general polynomial hyperelastic strain–energy function (Maher et al., 2009), single-term Ogden model (Barrett et al., 2009), neo-Hookean material (Chai et al., 2013; Holzapfel, 2000), Yeoh SEDF (Lawlor et al., 2011), Fung, Choi-Vito and modified Mooney–Rivlin SEDFs (Kural et al., 2012). As a fiber-oriented structure, considering the anisotropic behavior of atherosclerotic plaque it is essential for an accurate stress and strain prediction (Yang et al., 2009). However, current in vivo imaging techniques are unable to depict the fiber orientation within the plaque. With this in mind, isotropic material models may be more practical for clinically oriented studies.

The question therefore arises as to whether the stress prediction depends primarily on the constitutive law chosen or material constants involved. Fortunately, it seems that stress analysis can be used with confidence, as material properties variability generates relatively small errors in the prediction of wall stresses. Stresses within the arterial wall, fibrous plaque, calcified plaque, and lipid pool have low sensitivities for variation in the elastic modulus and material models. Even a $\pm50\%$ variation in elastic modulus leads to $<10\%$ change in stress at the site of rupture (Williamson et al., 2003). Sensitivity to variations in elastic modulus is comparable between isotropic nonlinear, isotropic nonlinear with residual strains and transversely isotropic linear models (Williamson et al., 2003). This was confirmed when the change in stress and strain values predicted, using parameters from two very different specimens, were relatively minor (within 20%) despite the substantial difference in stiffness and direction of anisotropy (Kural et al., 2012). However, such insensitivity may only stand under a certain circumstance and need further investigations. It was observed that for a thin FC (0.05 mm), the peak stress in a soft intima (Young's modulus: 33 kPa) was about 50% as intermediate (Young's modulus: 500 kPa) or stiff (Young's modulus: 1000 kPa) intima (Akyildiz et al., 2011).

4.2.2. Derived from in vivo measurements

Results from ex vivo direct measurements indicate that the constants describing the material properties of atherosclerotic tissues vary largely from study to study and from location to location, indicating the high non-homogeneity of tissues. Despite the reported insensitivity of material properties in stress prediction, a window may exist as stress and strain predictions can vary significantly if the variation of material properties/models exceeds a certain level (Yang et al., 2009). There is therefore still a need to obtain patient and location-specific material properties. Although this is a challenging goal, advancing imaging techniques may make it achievable. In this section material properties obtained with in vivo measurement are reviewed, particularly those obtained using elastography.

Elastography deals with calculation from elastograms and hence, begins with image registration, i.e., identify how each image point corresponding to a single material point of tissue that is moving within different frames. The gradient of the displacement field, computed in the registration step, generates the strain field (Ophir et al., 1991). For vascular application, the pulsatile intraluminal pressure is used as the deformation force. Ophir et al. (1991) first described the concept of strain imaging using ultrasound data, with the periodicity of ultrasound allowing accurate estimation of displacement. Due to the heterogeneous

nature of material stiffness within the atherosclerotic plaque, the displacement varies. Ultrasound-based elasticity imaging can portray such differences in the elastic properties of soft tissues. The accuracy of elastography in capturing deformation/strain has been widely assessed using phantom and finite element analysis (Allen et al., 2011; Dumont et al., 2011; Park et al., 2010; Ribbers et al., 2007). Its capacity in quantifying the material properties has been testified by comparing the results obtained in and ex vivo (Kanai et al., 2003; Viola et al., 2004; Xie et al., 2005). The technique has been employed widely to characterize plaque type (hard or soft) based on the displacement amplitude, allowing differentiation of vulnerable and stable lesions (Allen et al., 2011; Dahl et al., 2009; Schmitt et al., 2007).

With the assumption of linear elasticity, the material properties of arterial wall and atherosclerotic tissues in various artery beds have been investigated. In an ex vitro elastography study, average elasticity was 81 ± 40 kPa in the lipid region of 9 human iliac arteries and 1.0 ± 0.63 MPa where there was a mixture of smooth muscle and collagen fiber (Kanai et al., 2003). The difference between the obtained value in vivo and ex vivo was approximately 8%. In the same report, obtained from the in vivo data, the elasticity of healthy human common carotid artery was approximately 1 MPa ($n=2$) and that of lipid was about 100 kPa ($n=2$). Young's moduli for the common carotid artery were compared in groups with ($n=25$) and without (37) plaque (Paini et al., 2007). The value did not appear to significantly differ between groups (751 ± 560 kPa vs. 677 ± 427 kPa; $p > 0.05$). Based on in vivo cine and multi-contrast MR images, Liu et al. (2012) quantified material properties from 12 patients using modified Mooney–Rivlin SEDF. The effective Young's modulus varied from 137 kPa to 1435 kPa within the stretch range of [1.0, 1.3]. The non-linear material behavior of atherosclerotic tissues can also be captured with more sophisticated methods. Karimi et al. (2008) used a combination of non-linear finite element methods with a genetic algorithm to determine the material constants in the exponential form of the Mooney–Rivlin SEDF using optical coherence tomography images.

4.2.3. Material properties of plaque hemorrhage (PH)

Ultrasound-based elasticity imaging has also been used to capture the variation of Young's modulus of venous thrombosis in rats ($n=4$) during maturation (Aglyamov et al., 2007). The Young's modulus of venous thrombosis in rat, measured by in vivo elastography, increased from 8.53 ± 2.66 kPa at day 3 to 34.73 ± 8.26 kPa at day 10 ($n=12$) (Xie et al., 2005). The material properties of PH and intraluminal thrombus could be very similar considering their similar biological content. We have recently performed direct uni-axial material tests with PH and intraluminal thrombus, which demonstrate their non-linear material behavior. Modified Mooney–Rivlin SEDF was used to describe its stress–stretch relationship. In total, 12 PH tissue strips were obtained from CEA samples from 5 symptomatic patients. The fitted material constants were: c_1: 16.57×10^{-8} kPa [5.27×10^{-8}, 0.10]; D_1: 3.76 kPa [0.41, 2.67] and D_2: 8.90 [4.50, 12.44] (details of methodology are in the Appendix).

4.3. Shrinking procedure

In vivo plaque imaging, either from ultrasound, CT or MR, is acquired under pressurized conditions. The computational simulation should at least start from a zero pressure configuration due to the large deformation and non-linear material properties if the residual stress was ignored. Several techniques have been employed for this purpose. Inverse design analysis has been used in studies (Gee et al., 2009; Govindjee and Mihalic, 1996; Lu et al., 2007) to determine a truly stress-free configuration. A backward incremental method, which is a modified updated Lagrangian formulation, has also been applied to achieve a computational start shape in studies of abdominal aortic aneurysms (de Putter et al., 2007; Gee et al., 2009; Merkx et al., 2009; Speelman et al., 2009) and atherosclerotic plaques (Speelman et al., 2011). A pull-back algorithm was recently developed to determine the unloaded geometry in aneurysms (Riveros et al., 2013). These approaches lead to an acceptable recovery of vessel geometry with reasonable computational load. The uniform shrinkage method proposed by Huang et al. (2009) is an alternate approach (Tang et al., 2009a). It involves uniform shrinkage of the lumen contour about its geometric center before external loading is applied. The shrinkage rate is verified by comparing the pressurized geometry with the in vivo contour. Being a phenomenon-based technique, this is relatively easy to apply, but can fail to recover the in vivo configuration when the luminal shape is irregular. A non-uniform shrinking procedure has been proposed to handle this problem (Huang et al., 2011). It imposes further stretching in the major axis and compressing in the minor axis after the uniform shrinking. If the shrinking procedure is omitted, the stress prediction will be over-estimated in the plaque with a circular lumen shape (Tang et al., 2009a) and under-estimated in that with an irregular lumen shape (Huang et al., 2011).

4.4. Biomechanical stress analyses of carotid plaques with and without plaque hemorrhage (PH)

The association between mechanical loading and formation of plaque hemorrhage was proposed about 50 years ago. Constantinides (1967, 1984) suggested that FC microfissures could result from mechanical factors, such as bursts of hypertension or the constant bending and torsion of the arterial wall. The resulting effect could be the formation of an intraluminal thrombus; indeed FC erosion is thought to be responsible for approximately 40% of lethal coronary thromboses (Virmani et al., 2000). About 20 years later, Lusby et al. (1982b) proposed that mechanical/tensile stresses probably played an important role in the sudden transition from the asymptomatic to the symptomatic stage, most likely due to rupture of neovessels producing PH. It was also suggested that higher mechanical stresses could produce PH by stretching the intima and pushing the lesion further into the lumen. Due to limited numerical analysis techniques and computing power in the early 1980s, the tensile stress was approximated using Laplace's law. Since then only a few groups have studied this relationship. Compared to the worldwide interest in histological and imaging-based clinical studies on carotid plaque vulnerability, biomechanical analyses comprise only a fraction of the published research.

The association between neovessel rupture and mechanical loading was recently investigated by quantifying the mechanical conditions around each neovessel (Teng et al., 2012). It was found that neovessels with red blood cells nearby were subjected to a higher stretch level compared with those without red blood cells. High local stretch level may therefore lead to neovessel rupture, resulting in the formation and expansion of PH.

The association between PH and elevated stress at a patient level has also been explored. In a MRI-based study involving 45 symptomatic patients, the stress level over FC in 28 individuals with PH was significantly higher than those of asymptomatic patients (315 kPa [247–434] vs. 200 kPa [171–282]; $p=0.003$; median [inter quartile range]) (Sadat et al., 2011b). Similarly, Huang et al. (2010) performed 3D FSI on 5 patients showing that stress over FC near PH was higher than those locations without PH (75.6 kPa vs. 68.1 kPa; $p=0.0003$). The same group further reported that the size of PH had a significant impact on stress level over FC (Huang et al., 2012). The impact of hemorrhage evolution on the stress level over FC has also been explored. When the hemorrhage passes the acute period, stress decreased 30%

from 159 kPa [114–253] to 118 kPa [79–189] ($p=0.001$; $n=23$) (Sadat et al., 2011c). High stretch concentration around the rupture site in plaques with juxtaluminal hemorrhage (Teng et al., 2011) may prevent the plaque healing by inducing apoptosis of both smooth muscle and endothelial cells (Kainulainen et al., 2002; O'Brien et al., 1998). The peak stretch ratio in lesions with juxtaluminal hemorrhage was 2.10 ± 0.53 ($n=21$), which was significantly larger than lesions without such features (1.21 ± 0.08; $p < 0.0001$) (Teng et al., 2011). Large stretch may contribute to increasing plaque vulnerability, as 11 (11 out of 21 patients) recurrent events occurred in the first year in the patients with PH.

5. Expert commentary

PH is an important plaque component which significantly increases plaque vulnerability. Combined with other vulnerable plaque features, such as thin FC and large LRNC, it can form an important component towards more accurate patient risk stratification. Clinical studies have demonstrated the strong association between PH and future cerebrovascular events. Although biomechanical studies are few, they appear to support results of clinical studies. Advancements with in vivo imaging techniques, particularly MRI, have helped the investigation into the mechanisms and significance of PH. Determination of in vivo material properties for both PH and other plaque components would significantly assist patient-specific biomechanical simulations, hopefully leading to a refined risk assessment tool. However the complementary value provided by biomechanical analysis to the luminal stenosis and plaque morphological and compositional features in assessing plaque vulnerability needs further investigations. A collaborative effort by a multidisciplinary team of pathologists, radiologist, biomechanical engineers and clinicians is required to achieve this future goal.

Conflict of interest statement

Authors do not have any conflict of interest to be declared.

Acknowledgment

This research is supported by BHF PG/11/74/29100 and the NIHR Cambridge Biomedical Research Centre. Authors sincerely thank Dr. James Rudd and Dr. Francis Joshi for their permission of using the images in Fig. 2 (Department of Cardiovascular Medicine, University of Cambridge). We also thank Dr. Yuan Huang for his contribution in processing raw data of uni-axial test with PH and Dr. Chengcheng Zhu for providing MR images shown in Fig. 3 (Department of Radiology, University of Cambridge).

Appendix A. Supplementary material

Supplementary data associated with this article can be found in the online version at http://dx.doi.org/10.1016/j.jbiomech.2014.01.013.

References

AbuRahma, A.F., Boland, J.P., Robinson, P., Decanio, R., 1990. Antiplatelet therapy and carotid plaque hemorrhage and its clinical implications. J. Cardiovasc. Surg. (Torino) 31, 66–70.

Aglyamov, S.R., Skovoroda, A.R., Xie, H., Kim, K., Rubin, J.M., O'Donnell, M., Wakefield, T.W., Myers, D., Emelianov, S.Y., 2007. Model-based reconstructive elasticity imaging using ultrasound. Int. J. Biomed. Imaging 2007, 35830.

Ajduk, M., Pavic, L., Bulimbasic, S., Sarlija, M., Pavic, P., Patrlj, L., Brkljacic, B., 2009. Multidetector-row computed tomography in evaluation of atherosclerotic carotid plaques complicated with intraplaque hemorrhage. Ann. Vasc. Surg. 23, 186–193.

Akyildiz, A.C., Speelman, L., van Brummelen, H., Gutierrez, M.A., Virmani, R., van der Lugt, A., van der Steen, A.F., Wentzel, J.J., Gijsen, F.J., 2011. Effects of intima stiffness and plaque morphology on peak cap stress. BioMed. Eng. Online 10, 25.

Allen, J.D., Ham, K.L., Dumont, D.M., Sileshi, B., Trahey, G.E., Dahl, J.J., 2011. The development and potential of acoustic radiation force impulse (ARFI) imaging for carotid artery plaque characterization. Vasc. Med. 16, 302–311.

Altaf, N., Akwei, S., Auer, D.P., MacSweeney, S.T., Lowe, J., 2013. Magnetic resonance detected carotid plaque hemorrhage is associated with inflammatory features in symptomatic carotid plaques. Ann. Vasc. Surg. 27, 655–661.

Altaf, N., Daniels, L., Morgan, P.S., Auer, D., MacSweeney, S.T., Moody, A.R., Gladman, J.R., 2008. Detection of intraplaque hemorrhage by magnetic resonance imaging in symptomatic patients with mild to moderate carotid stenosis predicts recurrent neurological events. J. Vasc. Surg. 47, 337–342.

Altaf, N., MacSweeney, S.T., Gladman, J., Auer, D.P., 2007. Carotid intraplaque hemorrhage predicts recurrent symptoms in patients with high-grade carotid stenosis. Stroke 38, 1633–1635.

Ammar, A.D., Wilson, R.L., Travers, H., Lin, J.J., Farha, S.J., Chang, F.C., 1984. Intraplaque hemorrhage: its significance in cerebrovascular disease. Am. J. Surg. 148, 840–843.

Ammar, A.D., Ernst, R.L., Lin, J.J., Travers, H., 1986. The influence of repeated carotid plaque hemorrhages on the production of cerebrovascular symptoms. J. Vasc. Surg. 3, 857–859.

Arapoglou, B., Kondi-Pafiti, A., Katsenis, K., Dimakakos, P., 1994. The clinical significance of carotid plaque haemorrhage. Int. Angiol. 13, 323–326.

Balu, N., Yarnykh, V.L., Chu, B., Wang, J., Hatsukami, T., Yuan, C., 2011. Carotid plaque assessment using fast 3D isotropic resolution black-blood MRI. Magn. Reson. Med. 65, 627–637.

Balu, N., Yarnykh, V.L., Scholnick, J., Chu, B., Yuan, C., Hayes, C., 2009. Improvements in carotid plaque imaging using a new eight-element phased array coil at 3 T. J. Magn. Reson. Imaging 30, 1209–1214.

Barnett, H.J., Taylor, D.W., Eliasziw, M., Fox, A.J., Ferguson, G.G., Haynes, R.B., Rankin, R.N., Clagett, G.P., Hachinski, V.C., Sackett, D.L., Thorpe, K.E., Meldrum, H.E., Spence, J.D., 1998. Benefit of carotid endarterectomy in patients with symptomatic moderate or severe stenosis. North American Symptomatic Carotid Endarterectomy Trial Collaborators. N. Engl. J. Med. 339, 1415–1425.

Barrett, S.R., Sutcliffe, M.P., Howarth, S., Li, Z.Y., Gillard, J.H., 2009. Experimental measurement of the mechanical properties of carotid atherothrombotic plaque fibrous cap. J. Biomech. 42, 1650–1655.

Bassiouny, H.S., Davis, H., Massawa, N., Gewertz, B.L., Glagov, S., Zarins, C.K., 1989. Critical carotid stenoses: morphologic and chemical similarity between symptomatic and asymptomatic plaques. J. Vasc. Surg. 9, 202–212.

Bassiouny, H.S., Sakaguchi, Y., Mikucki, S.A., McKinsey, J.F., Piano, G., Gewertz, B.L., Glagov, S., 1997. Juxtalumenal location of plaque necrosis and neoformation in symptomatic carotid stenosis. J. Vasc. Surg. 26, 585–594.

Bitar, R., Moody, A.R., Leung, G., Symons, S., Crisp, S., Butany, J., Rowsell, C., Kiss, A., Nelson, A., Maggisano, R., 2008. In vivo 3D high-spatial-resolution MR imaging of intraplaque hemorrhage. Radiology 249, 259–267.

Bluestein, D., Alemu, Y., Avrahami, I., Gharib, M., Dumont, K., Ricotta, J.J., Einav, S., 2008. Influence of microcalcifications on vulnerable plaque mechanics using FSI modeling. J. Biomech. 41, 1111–1118.

Bornstein, N.M., Krajewski, A., Lewis, A.J., Norris, J.W., 1990. Clinical significance of carotid plaque hemorrhage. Arch. Neurol. 47, 958–959.

Carr, S., Farb, A., Pearce, W.H., Virmani, R., Yao, J.S., 1996. Atherosclerotic plaque rupture in symptomatic carotid artery stenosis. J. Vasc. Surg. 23, 755–765 (discussion 765-756).

Chai, C.K., Akyildiz, A.C., Speelman, L., Gijsen, F.J., Oomens, C.W., van Sambeek, M.R., van der Lugt, A., Baaijens, F.P., 2013. Local axial compressive mechanical properties of human carotid atherosclerotic plaques-characterisation by indentation test and inverse finite element analysis. J. Biomech. 46, 1759–1766.

Cheng, G.C., Loree, H.M., Kamm, R.D., Fishbein, M.C., Lee, R.T., 1993. Distribution of circumferential stress in ruptured and stable atherosclerotic lesions. A structural analysis with histopathological correlation. Circulation 87, 1179–1187.

Cheung, H.M., Moody, A.R., Singh, N., Bitar, R., Zhan, J., Leung, G., 2011. Late stage complicated atheroma in low-grade stenotic carotid disease: MR imaging depiction—prevalence and risk factors. Radiology 260, 841–847.

Chu, B., Kampschulte, A., Ferguson, M.S., Kerwin, W.S., Yarnykh, V.L., O'Brien, K.D., Polissar, N.L., Hatsukami, T.S., Yuan, C., 2004. Hemorrhage in the atherosclerotic carotid plaque: a high-resolution MRI study. Stroke 35, 1079–1084.

Coli, S., Magnoni, M., Sangiorgi, G., Marrocco-Trischitta, M.M., Melisurgo, G., Mauriello, A., Spagnoli, L., Chiesa, R., Cianflone, D., Maseri, A., 2008. Contrast-enhanced ultrasound imaging of intraplaque neovascularization in carotid arteries: correlation with histology and plaque echogenicity. J. Am. Coll. Cardiol. 52, 223–230.

Constantinides, P., 1967. Pathogenesis of cerebral artery thrombosis in man. Arch. Pathol. 83, 422–428.

Constantinides, P., 1984. Ultrastructural Pathobiology. Elsevier Science Publishers, Amsterdam

Dahl, J.J., Dumont, D.M., Allen, J.D., Miller, E.M., Trahey, G.E., 2009. Acoustic radiation force impulse imaging for noninvasive characterization of carotid artery atherosclerotic plaques: a feasibility study. Ultrasound Med. Biol. 35, 707–716.

Davies, M.J., Thomas, A.C., 1985. Plaque fissuring—the cause of acute myocardial infarction, sudden ischaemic death, and crescendo angina. Br. Heart J. 53, 363–373.
Delfino, A., Stergiopulos, N., Moore , J.E., Meister, J.J., 1997. Residual strain effects on the stress field in a thick wall finite element model of the human carotid bifurcation. J. Biomech. 30, 777–786.
Demarco, J.K., Ota, H., Underhill, H.R., Zhu, D.C., Reeves, M.J., Potchen, M.J., Majid, A., Collar, A., Talsma, J.A., Potru, S., Oikawa, M., Dong, L., Zhao, X., Yarnykh, V.L., Yuan, C., 2010. MR carotid plaque imaging and contrast-enhanced MR angiography identifies lesions associated with recent ipsilateral thromboembolic symptoms: an in vivo study at 3T. AJNR—Am. J. Neuroradiol. 31, 1395–1402.
Demos, S.M., Alkan-Onyuksel, H., Kane, B.J., Ramani, K., Nagaraj, A., Greene, R., Klegerman, M., McPherson, D.D., 1999. In vivo targeting of acoustically reflective liposomes for intravascular and transvascular ultrasonic enhancement. J. Am. Coll. Cardiol. 33, 867–875.
Derksen, W.J., Peeters, W., Tersteeg, C., de Vries, J.P., de Kleijn, D.P., Moll, F.L., van der Wal, A.C., Pasterkamp, G., Vink, A., 2011. Age and coumarin-type anticoagulation are associated with the occurrence of intraplaque hemorrhage, while statins are associated less with intraplaque hemorrhage: a large histopathological study in carotid and femoral plaques. Atherosclerosis 214, 139–143.
Dumont, D.M., Doherty, J.R., Trahey, G.E., 2011. Noninvasive assessment of wall-shear rate and vascular elasticity using combined ARFI/SWEI/spectral Doppler imaging system. Ultrason. Imaging 33, 165–188.
de Korte, C.L., Sierevogel, M.J., Mastik, F., Strijder, C., Schaar, J.A., Velema, E., Pasterkamp, G., Serruys, P.W., van der Steen, A.F., 2002. Identification of atherosclerotic plaque components with intravascular ultrasound elastography in vivo: a Yucatan pig study. Circulation 105, 1627–1630.
de Putter, S., Wolters, B.J., Rutten, M.C., Breeuwer, M., Gerritsen, F.A., van de Vosse, F.N., 2007. Patient-specific initial wall stress in abdominal aortic aneurysms with a backward incremental method. J. Biomech. 40, 1081–1090.
Ebenstein, D.M., Coughlin, D., Chapman, J., Li, C., Pruitt, L.A., 2009. Nanomechanical properties of calcification, fibrous tissue, and hematoma from atherosclerotic plaques. J. Biomed. Mater. Res. Part A 91, 1028–1037.
Eesa, M., Hill, M.D., Al-Khathaami, A., Al-Zawahmah, M., Sharma, P., Menon, B.K., Tymchuk, S., Demchuk, A.M., Goyal, M., 2010. Role of CT angiographic plaque morphologic characteristics in addition to stenosis in predicting the symptomatic side in carotid artery disease. AJNR—Am. J. Neuroradiol. 31, 1254–1260.
Eliasziw, M., Streifler, J.Y., Fox, A.J., Hachinski, V.C., Ferguson, G.G., Barnett, H.J., 1994. Significance of plaque ulceration in symptomatic patients with high-grade carotid stenosis. North American Symptomatic Carotid Endarterectomy Trial. Stroke 25, 304–308.
Feeley, T.M., Leen, E.J., Colgan, M.P., Moore, D.J., Hourihane, D.O., Shanik, G.D., 1991. Histologic characteristics of carotid artery plaque. J. Vasc. Surg. 13, 719–724.
Fisher, M., Jonas, S., Sacco, R.L., Jones, S., 1994. Prophylactic neuroprotection for cerebral ischemia. Stroke 25, 1075–1080.
Fryer, J.A., Myers, P.C., Appleberg, M., 1987. Carotid intraplaque hemorrhage: the significance of neovascularity. J. Vasc. Surg. 6, 341–349.
Fuster, V., 1994. Lewis A. Conner Memorial Lecture. Mechanisms leading to myocardial infarction: insights from studies of vascular biology. Circulation 90, 2126–2146.
Fuster, V., Fayad, Z.A., Moreno, P.R., Poon, M., Corti, R., Badimon, J.J., 2005. Atherothrombosis and high-risk plaque: Part II: approaches by noninvasive computed tomographic/magnetic resonance imaging. J. Am. Coll. Cardiol. 46, 1209–1218.
Gao, H., Long, Q., Graves, M., Gillard, J.H., Li, Z.Y., 2009. Study of reproducibility of human arterial plaque reconstruction and its effects on stress analysis based on multispectral in vivo magnetic resonance imaging. J. Magn. Reson. Imaging 30, 85–93.
Gao, P., Chen, Z.Q., Bao, Y.H., Jiao, L.Q., Ling, F., 2007. Correlation between carotid intraplaque hemorrhage and clinical symptoms: systematic review of observational studies. Stroke 38, 2382–2390.
Gatehouse, P.D., Keegan, J., Crowe, L.A., Masood, S., Mohiaddin, R.H., Kreitner, K.F., Firmin, D.N., 2005. Applications of phase-contrast flow and velocity imaging in cardiovascular MRI. Eur. Radiol. 15, 2172–2184.
Gee, M.W., Reeps, C., Eckstein, H.H., Wall, W.A., 2009. Prestressing in finite deformation abdominal aortic aneurysm simulation. J. Biomech. 42, 1732–1739.
Gortler, M., Goldmann, A., Mohr, W., Widder, B., 1995. Tissue characterisation of atherosclerotic carotid plaques by MRI. Neuroradiology 37, 631–635.
Govindjee, S., Mihalic, P., 1996. Computational methods for inverse finite elastostatics. Comput. Meth. Appl. Mech. Eng. 136, 47–57.
Grimm, J.M., Schindler, A., Freilinger, T., Cyran, C.C., Bamberg, F., Yuan, C., Reiser, M. F., Dichgans, M., Freilinger, C., Nikolaou, K., Saam, T., 2013. Comparison of symptomatic and asymptomatic atherosclerotic carotid plaques using parallel imaging and 3 T black-blood in vivo CMR. J. Cardiovasc. Magn. Reson. 15, 44.
Hellings, W.E., Peeters, W., Moll, F.L., Piers, S.R., van Setten, J., Van der Spek, P.J., de Vries, J.P., Seldenrijk, K.A., De Bruin, P.C., Vink, A., Velema, E., de Kleijn, D.P., Pasterkamp, G., 2010. Composition of carotid atherosclerotic plaque is associated with cardiovascular outcome: a prognostic study. Circulation 121, 1941–1950.
Holzapfel, G.A., 2000. Nonlinear Solid Mechanics. Wiley, Chicester, UK.
Horie, N., Morikawa, M., Ishizaka, S., Takeshita, T., So, G., Hayashi, K., Suyama, K., Nagata, I., 2012. Assessment of carotid plaque stability based on the dynamic enhancement pattern in plaque components with multidetector CT angiography. Stroke 43, 393–398.
Hosseini, A.A., Kandiyil, N., Macsweeney, S.T., Altaf, N., Auer, D.P., 2013. Carotid plaque hemorrhage on magnetic resonance imaging strongly predicts recurrent ischemia and stroke. Ann. Neurol. 73, 774–784.
Hu, X.B., Zhang, P.F., Su, H.J., Yi, X., Chen, L., Rong, Y.Y., Zhang, K., Li, X., Wang, L., Sun, C.L., Cai, X.J., Li, L., Song, J.T., Dai, X.M., Sui, X.D., Zhang, Y., Zhang, M., 2011. Intravascular ultrasound area strain imaging used to characterize tissue components and assess vulnerability of atherosclerotic plaques in a rabbit model. Ultrasound Med. Biol. 37, 1579–1587.
Huang, X., Teng, Z., Canton, G., Ferguson, M., Yuan, C., Tang, D., 2010. Intraplaque hemorrhage is associated with higher structural stresses in human atherosclerotic plaques: an in vivo MRI-based 3D fluid-structure interaction study. BioMed. Eng. Online 9, 86.
Huang, X., Yang, C., Canton, G., Ferguson, M., Yuan, C., Tang, D., 2012. Quantifying effect of intraplaque hemorrhage on critical plaque wall stress in human atherosclerotic plaques using three-dimensional fluid-structure interaction models. J. Biomech. Eng. 134, 121004.
Huang, X., Yang, C., Yuan, C., Liu, F., Canton, G., Zheng, J., Woodard, P.K., Sicard, G.A., Tang, D., 2009. Patient-specific artery shrinkage and 3D zero-stress state in multi-component 3D FSI models for carotid atherosclerotic plaques based on in vivo MRI data. Mol. Cell. Biomech. 6, 121–134.
Huang, Y., Teng, Z., Sadat, U., Hilborne, S., Young, V.E., Graves, M.J., Gillard, J.H., 2011. Non-uniform shrinkage for obtaining computational start shape for in-vivo MRI-based plaque vulnerability assessment. J. Biomech. 44, 2316–2319.
Imparato, A.M., Riles, T.S., Gorstein, F., 1979. The carotid bifurcation plaque: pathologic findings associated with cerebral ischemia. Stroke 10, 238–245.
Imparato, A.M., Riles, T.S., Mintzer, R., Baumann, F.G., 1983. The importance of hemorrhage in the relationship between gross morphologic characteristics and cerebral symptoms in 376 carotid artery plaques. Ann. Surg. 197, 195–203.
Jeziorska, M., Woolley, D.E., 1999. Neovascularization in early atherosclerotic lesions of human carotid arteries: its potential contribution to plaque development. Hum. Pathol. 30, 919–925.
Kainulainen, T., Pender, A., D'Addario, M., Feng, Y., Lekic, P., McCulloch, C.A., 2002. Cell death and mechanoprotection by filamin a in connective tissues after challenge by applied tensile forces. J. Biol. Chem. 277, 21998–22009.
Kampschulte, A., Ferguson, M.S., Kerwin, W.S., Polissar, N.L., Chu, B., Saam, T., Hatsukami, T.S., Yuan, C., 2004. Differentiation of intraplaque versus juxtaluminal hemorrhage/thrombus in advanced human carotid atherosclerotic lesions by in vivo magnetic resonance imaging. Circulation 110, 3239–3244.
Kanai, H., Hasegawa, H., Ichiki, M., Tezuka, F., Koiwa, Y., 2003. Elasticity imaging of atheroma with transcutaneous ultrasound: preliminary study. Circulation 107, 3018–3021.
Karimi, R., Zhu, T., Bouma, B.E., Mofrad, M.R., 2008. Estimation of nonlinear mechanical properties of vascular tissues via elastography. Cardiovasc. Eng. 8, 191–202.
Kiechl, S., Willeit, J., 1999. The natural course of atherosclerosis. Part I: incidence and progression. Arterioscler. Thromb. Vasc. Biol. 19, 1484–1490.
Kiousis, D.E., Rubinigg, S.F., Auer, M., Holzapfel, G.A., 2009. A methodology to analyze changes in lipid core and calcification onto fibrous cap vulnerability: the human atherosclerotic carotid bifurcation as an illustratory example. J. Biomech. Eng. 131, 121002.
Kock, S.A., Nygaard, J.V., Eldrup, N., Frund, E.T., Klaerke, A., Paaske, W.P., Falk, E., Yong Kim, W., 2008. Mechanical stresses in carotid plaques using MRI-based fluid–structure interaction models. J. Biomech. 41, 1651–1658.
Kolodgie, F.D., Gold, H.K., Burke, A.P., Fowler, D.R., Kruth, H.S., Weber, D.K., Farb, A., Guerrero, L.J., Hayase, M., Kutys, R., Narula, J., Finn, A.V., Virmani, R., 2003. Intraplaque hemorrhage and progression of coronary atheroma. N. Engl. J. Med. 349, 2316–2325.
Kural, M.H., Cai, M., Tang, D., Gwyther, T., Zheng, J., Billiar, K.L., 2012. Planar biaxial characterization of diseased human coronary and carotid arteries for computational modeling. J. Biomech. 45, 790–798.
Kurosaki, Y., Yoshida, K., Endo, H., Chin, M., Yamagata, S., 2011. Association between carotid atherosclerosis plaque with high signal intensity on T1-weighted imaging and subsequent ipsilateral ischemic events. Neurosurgery 68, 62–67 (discussion 67).
Kwee, R.M., Truijman, M.T., van Oostenbrugge, R.J., Mess, W.H., Prins, M.H., Franke, C.L., Korten, A.G., Wildberger, J.E., Kooi, M.E., 2012. Longitudinal MRI study on the natural history of carotid artery plaques in symptomatic patients. PLoS One 7, e42472.
Kwee, R.M., van Oostenbrugge, R.J., Mess, W.H., Prins, M.H., van der Geest, R.J., ter Berg, J.W., Franke, C.L., Korten, A.G., Meems, B.J., van Engelshoven, J.M., Wildberger, J.E., Kooi, M.E., 2010. Carotid plaques in transient ischemic attack and stroke patients: one-year follow-up study by magnetic resonance imaging. Investig. Radiol. 45, 803–809.
Kwee, R.M., van Oostenbrugge, R.J., Mess, W.H., Prins, M.H., van der Geest, R.J., ter Berg, J.W., Franke, C.L., Korten, A.G., Meems, B.J., van Engelshoven, J.M., Wildberger, J.E., Kooi, M.E., 2013. MRI of carotid atherosclerosis to identify TIA and stroke patients who are at risk of a recurrence. J. Magn. Reson. Imaging 37, 1189–1194.
Lawlor, M.G., O'Donnell, M.R., O'Connell, B.M., Walsh, M.T., 2011. Experimental determination of circumferential properties of fresh carotid artery plaques. J. Biomech. 44, 1709–1715.
Leach, J.R., Rayz, V.L., Soares, B., Wintermark, M., Mofrad, M.R., Saloner, D., 2010. Carotid atheroma rupture observed in vivo and FSI-predicted stress distribution based on pre-rupture imaging. Ann. Biomed. Eng. 38, 2748–2765.

Lennihan, L., Kupsky, W.J., Mohr, J.P., Hauser, W.A., Correll, J.W., Quest, D.O., 1987. Lack of association between carotid plaque hematoma and ischemic cerebral symptoms. Stroke 18, 879–881.
Levy, A.P., Moreno, P.R., 2006. Intraplaque hemorrhage. Curr. Mol. Med. 6, 479–488.
Levy, E.I., Mocco, J., Samuelson, R.M., Ecker, R.D., Jahromi, B.S., Hopkins, L.N., 2008. Optimal treatment of carotid artery disease. J. Am. Coll. Cardiol. 51, 979–985.
Li, F., Yarnykh, V.L., Hatsukami, T.S., Chu, B., Balu, N., Wang, J., Underhill, H.R., Zhao, X., Smith, R., Yuan, C., 2010. Scan-rescan reproducibility of carotid atherosclerotic plaque morphology and tissue composition measurements using multicontrast MRI at 3 T. J. Magn. Reson. Imaging 31, 168–176.
Lindner, J.R., Song, J., Xu, F., Klibanov, A.L., Singbartl, K., Ley, K., Kaul, S., 2000. Noninvasive ultrasound imaging of inflammation using microbubbles targeted to activated leukocytes. Circulation 102, 2745–2750.
Lindsay, A.C., Biasiolli, L., Lee, J.M., Kylintireas, I., MacIntosh, B.J., Watt, H., Jezzard, P., Robson, M.D., Neubauer, S., Handa, A., Kennedy, J., Choudhury, R.P., 2012. Plaque features associated with increased cerebral infarction after minor stroke and TIA: a prospective, case-control, 3-T carotid artery MR imaging study. JACC Cardiovasc. Imaging 5, 388–396.
Liu, H., Canton, G., Yuan, C., Yang, C., Billiar, K., Teng, Z., Hoffman, A.H., Tang, D., 2012. Using in vivo Cine and 3D multi-contrast MRI to determine human atherosclerotic carotid artery material properties and circumferential shrinkage rate and their impact on stress/strain predictions. J. Biomech. Eng. 134, 011008.
Long, Q., Xu, X.Y., Ariff, B., Thom, S.A., Hughes, A.D., Stanton, A.V., 2000. Reconstruction of blood flow patterns in a human carotid bifurcation: a combined CFD and MRI study. J. Magn. Reson. Imaging 11, 299–311.
Loree, H.M., Grodzinsky, A.J., Park, S.Y., Gibson, L.J., Lee, R.T., 1994. Static circumferential tangential modulus of human atherosclerotic tissue. J. Biomech. 27, 195–204.
Lu, J., Zhou, X., Raghavan, M.L., 2007. Inverse elastostatic stress analysis in predeformed biological structures: Demonstration using abdominal aortic aneurysms. J. Biomech. 40, 693–696.
Lusby, R.J., Ferrell, L.D., Ehrenfeld, W.K., Stoney, R.J., Wylie, E.J., 1982a. Carotid plaque hemorrhage. Its role in production of cerebral ischemia. Arch. Surg. 117, 1479–1488.
Lusby, R.J., Woodcock, J.P., Machleder, H.I., Ferrell, L.D., Jeans, W.D., Skidmore, R., Sheddon, E.J., Baird, R.N., 1982b. Transient ischaemic attacks: the static and dynamic morphology of the carotid artery bifurcation. Br. J. Surg. 69 (Suppl.), S41–S44.
Maher, E., Creane, A., Sultan, S., Hynes, N., Lally, C., Kelly, D.J., 2009. Tensile and compressive properties of fresh human carotid atherosclerotic plaques. J. Biomech. 42, 2760–2767.
McCarthy, M.J., Loftus, I.M., Thompson, M.M., Jones, L., London, N.J., Bell, P.R., Naylor, A.R., Brindle, N.P., 1999. Angiogenesis and the atherosclerotic carotid plaque: an association between symptomatology and plaque morphology. J. Vasc. Surg. 30, 261–268.
Merkx, M.A., van't Veer, M., Speelman, L., Breeuwer, M., Buth, J., van de Vosse, F.N., 2009. Importance of initial stress for abdominal aortic aneurysm wall motion: dynamic MRI validated finite element analysis. J. Biomech. 42, 2369–2373.
Michel, J.B., Delbosc, S., Ho-Tin-Noe, B., Leseche, G., Nicoletti, A., Meilhac, O., Martin-Ventura, J.L., 2012. From intraplaque haemorrhages to plaque vulnerability: biological consequences of intraplaque haemorrhages. J. Cardiovasc. Med. (Hagerstown) 13, 628–634.
Michel, J.B., Virmani, R., Arbustini, E., Pasterkamp, G., 2011. Intraplaque haemorrhages as the trigger of plaque vulnerability. Eur. Heart J. 32, 1977–1985 (1985a, 1985b, 1985c).
Milei, J., Parodi, J.C., Alonso, G.F., Barone, A., Grana, D., Matturri, L., 1998. Carotid rupture and intraplaque hemorrhage: immunophenotype and role of cells involved. Am. Heart. J. 136, 1096–1105.
Milei, J., Parodi, J.C., Ferreira, M., Barrone, A., Grana, D.R., Matturri, L., 2003. Atherosclerotic plaque rupture and intraplaque hemorrhage do not correlate with symptoms in carotid artery stenosis. J. Vasc. Surg. 38, 1241–1247.
Millon, A., Mathevet, J.L., Boussel, L., Faries, P.L., Fayad, Z.A., Douek, P.C., Feugier, P., 2013. High-resolution magnetic resonance imaging of carotid atherosclerosis identifies vulnerable carotid plaques. J. Vasc. Surg. 57, 1046–1051 (e1042).
Montauban van Swijndregt, A.D., Elbers, H.R., Moll, F.L., de Letter, J., Ackerstaff, R.G., 1999. Cerebral ischemic disease and morphometric analyses of carotid plaques. Ann. Vasc. Surg. 13, 468–474.
Moody, A.R., Murphy, R.E., Morgan, P.S., Martel, A.L., Delay, G.S., Allder, S., MacSweeney, S.T., Tennant, W.G., Gladman, J., Lowe, J., Hunt, B.J., 2003. Characterization of complicated carotid plaque with magnetic resonance direct thrombus imaging in patients with cerebral ischemia. Circulation 107, 3047–3052.
Moreno, P.R., Purushothaman, M., Purushothaman, K.R., 2012. Plaque neovascularization: defense mechanisms, betrayal, or a war in progress. Ann. N. Y. Acad. Sci. 1254, 7–17.
Mugler , J.P., Brookeman, J.R., 1990. Three-dimensional magnetization-prepared rapid gradient-echo imaging (3D MP RAGE). Magn. Reson. Med. 15, 152–157.
O'Brien , J.E., Ormont, M.L., Shi, Y., Wang, D., Zalewski, A., Mannion, J.D., 1998. Early injury to the media after saphenous vein grafting. Ann. Thorac. Surg. 65, 1273–1278.
Ohayon, J., Dubreuil, O., Tracqui, P., Le Floc'h, S., Rioufol, G., Chalabreysse, L., Thivolet, F., Pettigrew, R.I., Finet, G., 2007. Influence of residual stress/strain on the biomechanical stability of vulnerable coronary plaques: potential impact for evaluating the risk of plaque rupture. Am. J. Physiol. Heart Circ. Physiol. 293, H1987–H1996.
Ophir, J., Cespedes, I., Ponnekanti, H., Yazdi, Y., Li, X., 1991. Elastography: a quantitative method for imaging the elasticity of biological tissues. Ultrason. Imaging 13, 111–134.
Ota, H., Yarnykh, V.L., Ferguson, M.S., Underhill, H.R., Demarco, J.K., Zhu, D.C., Oikawa, M., Dong, L., Zhao, X., Collar, A., Hatsukami, T.S., Yuan, C., 2010. Carotid intraplaque hemorrhage imaging at 3.0-T MR imaging: comparison of the diagnostic performance of three T1-weighted sequences. Radiology 254, 551–563.
Paini, A., Boutouyrie, P., Calvet, D., Zidi, M., Agabiti-Rosei, E., Laurent, S., 2007. Multiaxial mechanical characteristics of carotid plaque: analysis by multiarray echotracking system. Stroke 38, 117–123.
Papaioannou, T.G., Protogerou, A.D., Stamatelopoulos, K.S., Vavuranakis, M., Stefanadis, C., 2009. Non-invasive methods and techniques for central blood pressure estimation: procedures, validation, reproducibility and limitations. Curr. Pharm. Des. 15, 245–253.
Park, D.W., Richards, M.S., Rubin, J.M., Hamilton, J., Kruger, G.H., Weitzel, W.F., 2010. Arterial elasticity imaging: comparison of finite-element analysis models with high-resolution ultrasound speckle tracking. Cardiovasc. Ultrasound 8, 22.
Paterson, J., 1938. Capillary rupture with intimal hemorrhage as a causative factor in coronary thrombus. Arch. Pathol. Lab. Med. 474–487
Paterson, J.C., 1936. Vascularization and hemorrhage of the intima of coronary atherosclerotic arteries. Arch. Pathol. 22, 312–324.
Persson, A.V., Robichaux, W.T., Silverman, M., 1983. The natural history of carotid plaque development. Arch. Surg. 118, 1048–1052.
Persson, A.V., 1986. Intraplaque hemorrhage. Surg. Clin. North Am. 66, 415–420.
Qiao, Y., Etesami, M., Malhotra, S., Astor, B.C., Virmani, R., Kolodgie, F.D., Trout , H.H., Wasserman, B.A., 2011. Identification of intraplaque hemorrhage on MR angiography images: a comparison of contrast-enhanced mask and time-of-flight techniques. AJNR—Am. J. Neuroradiol. 32, 454–459.
Qiao, Y., Etesami, M., Astor, B.C., Zeiler, S.R., Trout , H.H., Wasserman, B.A., 2012. Carotid plaque neovascularization and hemorrhage detected by MR imaging are associated with recent cerebrovascular ischemic events. AJNR—Am. J. Neuroradiol. 33, 755–760.
Reilly, L.M., Lusby, R.J., Hughes, L., Ferrell, L.D., Stoney, R.J., Ehrenfeld, W.K., 1983. Carotid plaque histology using real-time ultrasonography. Clinical and therapeutic implications. Am. J. Surg. 146, 188–193.
Ribbers, H., Lopata, R.G., Holewijn, S., Pasterkamp, G., Blankensteijn, J.D., de Korte, C. L., 2007. Noninvasive two-dimensional strain imaging of arteries: validation in phantoms and preliminary experience in carotid arteries in vivo. Ultrasound Med. Biol. 33, 530–540.
Riveros, F., Chandra, S., Finol, E.A., Gasser, T.C., Rodriguez, J.F., 2013. A pull-back algorithm to determine the unloaded vascular geometry in anisotropic hyperelastic AAA passive mechanics. Ann. Biomed. Eng. 41, 694–708.
Ricotta, J.J., Schenk, E.A., Ekholm, S.E., DeWeese, J.A., 1986. Angiographic and pathologic correlates in carotid artery disease. Surgery 99, 284–292.
Roger, V.L., Go, A.S., Lloyd-Jones, D.M., Adams, R.J., Berry, J.D., Brown, T.M., Carnethon, M.R., Dai, S., de Simone, G., Ford, E.S., Fox, C.S., Fullerton, H.J., Gillespie, C., Greenlund, K.J., Hailpern, S.M., Heit, J.A., Ho, P.M., Howard, V.J., Kissela, B.M., Kittner, S.J., Lackland, D.T., Lichtman, J.H., Lisabeth, L.D., Makuc, D. M., Marcus, G.M., Marelli, A., Matchar, D.B., McDermott, M.M., Meigs, J.B., Moy, C.S., Mozaffarian, D., Mussolino, M.E., Nichol, G., Paynter, N.P., Rosamond, W.D., Sorlie, P.D., Stafford, R.S., Turan, T.N., Turner, M.B., Wong, N.D., Wylie-Rosett, J., 2011. Heart disease and stroke statistics—2011 update: a report from the American Heart Association. Circulation 123, e18–e209.
Rothwell, P.M., Gibson, R., Warlow, C.P., 2000. On behalf of the European Carotid Surgery Trialists' Collaborative Group, 2000. Interrelation between plaque surface morphology and degree of stenosis on carotid angiograms and the risk of ischemic stroke in patients with symptomatic carotid stenosis. Stroke 31, 615–621.
Rothwell, P.M., Gutnikov, S.A., Warlow, C.P., 2003. Reanalysis of the final results of the European Carotid Surgery Trial. Stroke 34, 514–523.
Saam, T., Cai, J., Ma, L., Cai, Y.Q., Ferguson, M.S., Polissar, N.L., Hatsukami, T.S., Yuan, C., 2006. Comparison of symptomatic and asymptomatic atherosclerotic carotid plaque features with in vivo MR imaging. Radiology 240, 464–472.
Saba, L., Caddeo, G., Sanfilippo, R., Montisci, R., Mallarini, G., 2007. CT and ultrasound in the study of ulcerated carotid plaque compared with surgical results: potentialities and advantages of multidetector row CT angiography. AJNR—Am. J. Neuroradiol. 28, 1061–1066.
Sadat, U., Teng, Z., Gillard, J.H., 2010a. Biomechanical structural stresses of atherosclerotic plaques. Expert Rev. Cardiovasc. Ther. 8, 1469–1481.
Sadat, U., Teng, Z., Young, V.E., Walsh, S.R., Li, Z.Y., Graves, M.J., Varty, K., Gillard, J.H., 2010b. Association between biomechanical structural stresses of atherosclerotic carotid plaques and subsequent ischaemic cerebrovascular events—a longitudinal in vivo magnetic resonance imaging-based finite element study. Eur. J. Vasc. Endovasc. Surg. 40, 485–491.
Sadat, U., Teng, Z., Young, V.E., Walsh, S.R., Li, Z.Y., Graves, M.J., Varty, K., Gillard, J.H., 2010c. Association between biomechanical structural stresses of atherosclerotic carotid plaques and subsequent ischaemic cerebrovascular events—a longitudinal in vivo magnetic resonance imaging-based finite element study. Eur. J. Vasc. Endovasc. Surg.
Sadat, U., Teng, Z., Young, V.E., Graves, M.J., Gaunt, M.E., Gillard, J.H., 2011a. High-resolution magnetic resonance imaging-based biomechanical stress analysis of carotid atheroma: a comparison of single transient ischaemic attack, recurrent transient ischaemic attacks, non-disabling stroke and asymptomatic patient groups. Eur. J. Vasc. Endovasc. Surg. 41, 83–90.

Sadat, U., Teng, Z., Young, V.E., Li, Z.Y., Gillard, J.H., 2011b. Utility of magnetic resonance imaging-based finite element analysis for the biomechanical stress analysis of hemorrhagic and non-hemorrhagic carotid plaques. Circ. J. 75, 884–889.
Sadat, U., Teng, Z., Young, V.E., Zhu, C., Tang, T.Y., Graves, M.J., Gillard, J.H., 2011c. Impact of plaque haemorrhage and its age on structural stresses in atherosclerotic plaques of patients with carotid artery disease: an MR imaging-based finite element simulation study. Int. J. Cardiovasc. Imaging 27, 397–402.
Sadat, U., Weerakkody, R.A., Bowden, D.J., Young, V.E., Graves, M.J., Li, Z.Y., Tang, T.Y., Gaunt, M.E., Hayes, P.D., Gillard, J.H., 2009. Utility of high resolution MR imaging to assess carotid plaque morphology: a comparison of acute symptomatic, recently symptomatic and asymptomatic patients with carotid artery disease. Atherosclerosis 207, 434–439.
Schmitt, C., Soulez, G., Maurice, R.L., Giroux, M.F., Cloutier, G., 2007. Noninvasive vascular elastography: toward a complementary characterization tool of atherosclerosis in carotid arteries. Ultrasound Med. Biol. 33, 1841–1858.
Schulze-Bauer, C.A., Holzapfel, G.A., 2003. Determination of constitutive equations for human arteries from clinical data. J. Biomech. 36, 165–169.
Seeger, J.M., Barratt, E., Lawson, G.A., Klingman, N., 1995. The relationship between carotid plaque composition, plaque morphology, and neurologic symptoms. J. Surg. Res. 58, 330–336.
Shi, H., Mitchell, C.C., McCormick, M., Kliewer, M.A., Dempsey, R.J., Varghese, T., 2008. Preliminary in vivo atherosclerotic carotid plaque characterization using the accumulated axial strain and relative lateral shift strain indices. Phys. Med. Biol. 53, 6377–6394.
Siebenhofer, A., Kemp, C., Sutton, A., Williams, B., 1999. The reproducibility of central aortic blood pressure measurements in healthy subjects using applanation tonometry and sphygmocardiography. J. Hum. Hypertens. 13, 625–629.
Singh, N., Moody, A.R., Gladstone, D.J., Leung, G., Ravikumar, R., Zhan, J., Maggisano, R., 2009. Moderate carotid artery stenosis: MR imaging-depicted intraplaque hemorrhage predicts risk of cerebrovascular ischemic events in asymptomatic men. Radiology 252, 502–508.
Sitzer, M., Muller, W., Siebler, M., Hort, W., Kniemeyer, H.W., Jancke, L., Steinmetz, H., 1995. Plaque ulceration and lumen thrombus are the main sources of cerebral microemboli in high-grade internal carotid artery stenosis. Stroke 26, 1231–1233.
Sommer, G., Regitnig, P., Koltringer, L., Holzapfel, G.A., 2010. Biaxial mechanical properties of intact and layer-dissected human carotid arteries at physiological and supraphysiological loadings. Am. J. Physiol. Heart Circ. Physiol. 298, H898–H912.
Spagnoli, L.G., Mauriello, A., Sangiorgi, G., Fratoni, S., Bonanno, E., Schwartz, R.S., Piepgras, D.G., Pistolese, R., Ippoliti, A., Holmes , D.R., 2004. Extracranial thrombotically active carotid plaque as a risk factor for ischemic stroke. J. Am. Med. Assoc. 292, 1845–1852.
Speelman, L., Akyildiz, A.C., den Adel, B., Wentzel, J.J., van der Steen, A.F., Virmani, R., van der Weerd, L., Jukema, J.W., Poelmann, R.E., van Brummelen, E.H., Gijsen, F.J., 2011. Initial stress in biomechanical models of atherosclerotic plaques. J. Biomech. 44, 2376–2382.
Speelman, L., Bosboom, E.M., Schurink, G.W., Buth, J., Breeuwer, M., Jacobs, M.J., van de Vosse, F.N., 2009. Initial stress and nonlinear material behavior in patient-specific AAA wall stress analysis. J. Biomech. 42, 1713–1719.
Sterpetti, A.V., Hunter, W.J., Schultz, R.D., 1991. Importance of ulceration of carotid plaque in determining symptoms of cerebral ischemia. J. Cardiovasc. Surg. (Torino) 32, 154–158.
Sun, J., Balu, N., Hippe, D.S., Xue, Y., Dong, L., Zhao, X., Li, F., Xu, D., Hatsukami, T.S., Yuan, C., 2013. Subclinical carotid atherosclerosis: short-term natural history of lipid-rich necrotic core—a multicenter study with MR imaging. Radiology 268, 61–68.
Sun, J., Underhill, H.R., Hippe, D.S., Xue, Y., Yuan, C., Hatsukami, T.S., 2012. Sustained acceleration in carotid atherosclerotic plaque progression with intraplaque hemorrhage: a long-term time course study. JACC Cardiovasc. Imaging 5, 798–804.
Takaya, N., Yuan, C., Chu, B., Saam, T., Polissar, N.L., Jarvik, G.P., Isaac, C., McDonough, J., Natiello, C., Small, R., Ferguson, M.S., Hatsukami, T.S., 2005. Presence of intraplaque hemorrhage stimulates progression of carotid atherosclerotic plaques: a high-resolution magnetic resonance imaging study. Circulation 111, 2768–2775.
Takaya, N., Yuan, C., Chu, B., Saam, T., Underhill, H., Cai, J., Tran, N., Polissar, N.L., Isaac, C., Ferguson, M.S., Garden, G.A., Cramer, S.C., Maravilla, K.R., Hashimoto, B., Hatsukami, T.S., 2006. Association between carotid plaque characteristics and subsequent ischemic cerebrovascular events: a prospective assessment with MRI—initial results. Stroke 37, 818–823.
Tang, D., Teng, Z., Canton, G., Hatsukami, T.S., Dong, L., Huang, X., Yuan, C., 2009a. Local critical stress correlates better than global maximum stress with plaque morphological features linked to atherosclerotic plaque vulnerability: an in vivo multi-patient study. BioMed. Eng. Online 8, 15.
Tang, D., Teng, Z., Canton, G., Yang, C., Ferguson, M., Huang, X., Zheng, J., Woodard, P.K., Yuan, C., 2009b. Sites of rupture in human atherosclerotic carotid plaques are associated with high structural stresses: an in vivo MRI-based 3D fluid–structure interaction study. Stroke 40, 3258–3263.
Tegos, T.J., Sohail, M., Sabetai, M.M., Robless, P., Akbar, N., Pare, G., Stansby, G., Nicolaides, A.N., 2000. Echomorphologic and histopathologic characteristics of unstable carotid plaques. AJNR—Am. J. Neuroradiol. 21, 1937–1944.
Teng, Z., He, J., Degnan, A.J., Chen, S., Sadat, U., Bahaei, N.S., Rudd, J.H., Gillard, J.H., 2012. Critical mechanical conditions around neovessels in carotid atherosclerotic plaque may promote intraplaque hemorrhage. Atherosclerosis 223, 321–326.
Teng, Z., Sadat, U., Huang, Y., Young, V.E., Graves, M.J., Lu, J., Gillard, J.H., 2011. In vivo MRI-based 3D mechanical stress–strain profiles of carotid plaques with juxtaluminal plaque haemorrhage: an exploratory study for the mechanism of subsequent cerebrovascular events. Eur. J. Vasc. Endovasc. Surg. 42, 427–433.
Thrysoe, S.A., Oikawa, M., Yuan, C., Eldrup, N., Klaerke, A., Paaske, W.P., Falk, E., Kim, W.Y., Nygaard, J.V., 2010. Longitudinal distribution of mechanical stresses in carotid plaques of symptomatic patients. Stroke 41, 1041–1043.
Tong, J., Sommer, G., Regitnig, P., Holzapfel, G.A., 2011. Dissection properties and mechanical strength of tissue components in human carotid bifurcations. Ann. Biomed. Eng. 39, 1703–1719.
Toussaint, J.F., LaMuraglia, G.M., Southern, J.F., Fuster, V., Kantor, H.L., 1996. Magnetic resonance images lipid, fibrous, calcified, hemorrhagic, and thrombotic components of human atherosclerosis in vivo. Circulation 94, 932–938.
Trivedi, R.A., J, U.K.-I., Graves, M.J., Horsley, J., Goddard, M., Kirkpatrick, P.J., Gillard, J. H., 2004. Multi-sequence in vivo MRI can quantify fibrous cap and lipid core components in human carotid atherosclerotic plaques. Eur. J. Vasc. Endovasc. Surg. 28, 207–213.
Turc, G., Oppenheim, C., Naggara, O., Eker, O.F., Calvet, D., Lacour, J.C., Crozier, S., Guegan-Massardier, E., Henon, H., Neau, J.P., Toussaint, J.F., Mas, J.L., Meder, J.F., Touze, E., 2012. Relationships between recent intraplaque hemorrhage and stroke risk factors in patients with carotid stenosis: the HIRISC study. Arterioscler. Thromb. Vasc. Biol. 32, 492–499.
Turu, M.M., Krupinski, J., Catena, E., Rosell, A., Montaner, J., Rubio, F., Alvarez-Sabin, J., Cairols, M., Badimon, L., 2006. Intraplaque MMP-8 levels are increased in asymptomatic patients with carotid plaque progression on ultrasound. Atherosclerosis 187, 161–169.
U-King-Im, J.M., Tang, T.Y., Patterson, A., Graves, M., Howard, S., Li, Z.Y., Trivedi, R., Browden, D., Kirkpatrick, P.J., Gaunt, M.E., Warburton, E.A., Antoun, N.M., Gillard, J.H., 2008. Characterisation of carotid atheroma in symptomatic and asymptomatic patients using high resolution MRI. J. Neurol. Neurosurg. Psychiatry 79, 905–912.
U-King-Im, J.M., Young, V., Gillard, J.H., 2009. Carotid-artery imaging in the diagnosis and management of patients at risk of stroke. Lancet Neurol. 8, 569–580.
U-King-Im, J.M., Fox, A.J., Aviv, R.I., Howard, P., Yeung, R., Moody, A.R., Symons, S.P., 2010. Characterization of carotid plaque hemorrhage: a CT angiography and MR intraplaque hemorrhage study. Stroke 41, 1623–1629.
Underhill, H.R., Hatsukami, T.S., Fayad, Z.A., Fuster, V., Yuan, C., 2010. MRI of carotid atherosclerosis: clinical implications and future directions. Nat. Rev. Cardiol. 7, 165–173.
Vicenzini, E., Giannoni, M.F., Puccinelli, F., Ricciardi, M.C., Altieri, M., Di Piero, V., Gossetti, B., Valentini, F.B., Lenzi, G.L., 2007. Detection of carotid adventitial vasa vasorum and plaque vascularization with ultrasound cadence contrast pulse sequencing technique and echo-contrast agent. Stroke 38, 2841–2843.
Viola, F., Kramer, M.D., Lawrence, M.B., Oberhauser, J.P., Walker, W.F., 2004. Sonorheometry: a noncontact method for the dynamic assessment of thrombosis. Ann. Biomed. Eng. 32, 696–705.
Virmani, R., Kolodgie, F.D., Burke, A.P., Farb, A., Schwartz, S.M., 2000. Lessons from sudden coronary death: a comprehensive morphological classification scheme for atherosclerotic lesions. Arterioscler. Thromb. Vasc. Biol. 20, 1262–1275.
Virmani, R., Kolodgie, F.D., Burke, A.P., Finn, A.V., Gold, H.K., Tulenko, T.N., Wrenn, S.P., Narula, J., 2005. Atherosclerotic plaque progression and vulnerability to rupture: angiogenesis as a source of intraplaque hemorrhage. Arterioscler. Thromb. Vasc. Biol. 25, 2054–2061.
von Maravic, C., Kessler, C., von Maravic, M., Hohlbach, G., Kompf, D., 1991. Clinical relevance of intraplaque hemorrhage in the internal carotid artery. Eur. J. Surg. 157, 185–188.
Walker, L.J., Ismail, A., McMeekin, W., Lambert, D., Mendelow, A.D., Birchall, D., 2002. Computed tomography angiography for the evaluation of carotid atherosclerotic plaque: correlation with histopathology of endarterectomy specimens. Stroke 33, 977–981.
Wang, J., Bornert, P., Zhao, H., Hippe, D.S., Zhao, X., Balu, N., Ferguson, M.S., Hatsukami, T.S., Xu, J., Yuan, C., Kerwin, W.S., 2013. Simultaneous noncontrast angiography and intraplaque hemorrhage (SNAP) imaging for carotid atherosclerotic disease evaluation. Magn. Reson. Med. 69, 337–345.
Wang, J., Ferguson, M.S., Balu, N., Yuan, C., Hatsukami, T.S., Bornert, P., 2010. Improved carotid intraplaque hemorrhage imaging using a slab-selective phase-sensitive inversion-recovery (SPI) sequence. Magn. Reson. Med. 64, 1332–1340.
Wartman, W.B., 1938. Occlusion of the coronary arteries by hemorrhage into their walls. Am. Heart. J. 459–470
Williamson, S.D., Lam, Y., Younis, H.F., Huang, H., Patel, S., Kaazempur-Mofrad, M.R., Kamm, R.D., 2003. On the sensitivity of wall stresses in diseased arteries to variable material properties. J. Biomech. Eng. 125, 147–155.
Xie, H., Kim, K., Aglyamov, S.R., Emelianov, S.Y., O'Donnell, M., Weitzel, W.F., Wrobleski, S.K., Myers, D.D., Wakefield, T.W., Rubin, J.M., 2005. Correspondence of ultrasound elasticity imaging to direct mechanical measurement in aging DVT in rats. Ultrasound. Med. Biol. 31, 1351–1359.
Yamada, K., Song, Y., Hippe, D.S., Sun, J., Dong, L., Xu, D., Ferguson, M.S., Chu, B., Hatsukami, T.S., Chen, M., Zhou, C., Yuan, C., 2012. Quantitative evaluation of high intensity signal on MIP images of carotid atherosclerotic plaques from routine TOF-MRA reveals elevated volumes of intraplaque hemorrhage and lipid rich necrotic core. J. Cardiovasc. Magn. Reson. 14, 81.
Yang, C., Bach, R.G., Zheng, J., Naqa, I.E., Woodard, P.K., Teng, Z., Billiar, K., Tang, D., 2009. In vivo IVUS-based 3-D fluid–structure interaction models with cyclic

bending and anisotropic vessel properties for human atherosclerotic coronary plaque mechanical analysis. IEEE Trans. Biomed. Eng. 56, 2420–2428.
Yim, Y.J., Choe, Y.H., Ko, Y., Kim, S.T., Kim, K.H., Jeon, P., Byun, H.S., Kim, D.I., 2008. High signal intensity halo around the carotid artery on maximum intensity projection images of time-of-flight MR angiography: a new sign for intraplaque hemorrhage. J. Magn. Reson. Imaging 27, 1341–1346.
Yoshida K., Sadamasa N., Narumi O., Chin M., Yamagata S., Miyamoto S., 2012. Symptomatic low-grade carotid stenosis with intraplaque hemorrhage and expansive arterial remodeling is associated with a high relapse rate refractory to medical treatment. Neurosurgery 70, 1143-1150; discussion 1150-1141.
Yuan, C., Mitsumori, L.M., Ferguson, M.S., Polissar, N.L., Echelard, D., Ortiz, G., Small, R., Davies, J.W., Kerwin, W.S., Hatsukami, T.S., 2001. In vivo accuracy of multispectral magnetic resonance imaging for identifying lipid-rich necrotic cores and intraplaque hemorrhage in advanced human carotid plaques. Circulation 104, 2051–2056.
Zachrisson, H., Engstrom, E., Engvall, J., Wigstrom, L., Smedby, O., Persson, A., 2010. Soft tissue discrimination ex vivo by dual energy computed tomography. Eur. J. Radiol. 75, e124–e128.
Zhang, L., Liu, Y., Zhang, P.F., Zhao, Y.X., Ji, X.P., Lu, X.T., Chen, W.Q., Liu, C.X., Zhang, C., Zhang, Y., 2010a. Peak radial and circumferential strain measured by velocity vector imaging is a novel index for detecting vulnerable plaques in a rabbit model of atherosclerosis. Atherosclerosis 211, 146–152.
Zhang, P.F., Su, H.J., Zhang, M., Li, J.F., Liu, C.X., Ding, S.F., Miao, Y., Chen, L., Li, X.N., Yi, X., Zhang, Y., 2010b. Atherosclerotic plaque components characterization and macrophage infiltration identification by intravascular ultrasound elastography based on b-mode analysis: validation in vivo. Int. J. Cardiovasc. Imaging 27, 39–49.
Zhu, D.C., Vu, A.T., Ota, H., DeMarco, J.K., 2010. An optimized 3D spoiled gradient recalled echo pulse Sequence for Hemorrhage assessment using INversion recovery and multiple Echoes (3D SHINE) for carotid plaque imaging. Magn. Reson. Med. 64, 1341–1351.